Faculty and Researchers	Faculty and Researchers' Publications

Computer Simulation of Pit Formation in Metals by Ion Bombardment

Webb, R.P.; Harrison, D.E.

Computer Simulation of Pit Formation in Metals by Ion Bombardment

R. P. Webb and D. E. Harrison, Jr.

Naval Postgraduate School, Monterey, California 93940

Computer simulations of ion-bombardment events which recrystallize the target demonstrate pit formation at 1.0 keV. Atoms are ejected from the first two target layers in the pit region. The remainder of the pit is created by replacement-collision sequences. Linear-cascade and spike-regime events are dynamically indistinguishable.

Small craterlike pits are observable, near the limit of resolution of the transmission electron microscope (TEM), in metal surfaces which have been bombarded by heavy high-energy ions.[1] Because they are seen in experimental systems where high-energy-density cascades are to be expected,[1-3] pits have been interpreted as evidence for spike effects[4,5] and as indicators of the breakdown of linear cascade theory. On the assumption that atoms are ejected from these pits, Merkle and Jager[1] proposed a model which correlates pit volume with the sputtering yield.

Multiple-interaction molecular-dynamics simulations show that for ion energies less than 20 keV most ejected atoms come from the surface layer of the target.[6] This result recently has been confirmed experimentally for ion energies up to 25.0 keV for a liquid-Ga-In/Ar^+ system.[7] When taken in conjunction with the pit results, these simulations and experiments seem to confirm that sputtering processes are different in the high-energy-density–cascade and the linear-cascade regimes.

Detailed analyses of individual trajectories indicate that this is not the case. In the simulations pits have been recorded for ion energies from 1.0 to 20.0 keV in the model system studied. Relatively low-energy ions produce pits when the energy they deposit in the surface region greatly exceeds the average value obtained from linear cascade theory. The maximum observed pit size increases with the ion energy.

The sputtering simulation program has been described in the literature.[8-11] For this analysis a cooling process, which will be described in detail elsewhere,[12] has been added to the basic model. In brief, the cooling code removes energy from the final ion-induced amorphous region in a manner analogous to the dissipation of energy from a "thermal spike" via phonon processes,[13] using a logic developed to study the relaxation of atoms around point defects.[14] Most spatial relationships between atoms, developed during the

collision cascade, are retained as the target coalesces, but some atoms move short distances. The details of a perfect recrystallization model are not required here because exact atomic positions are not required when only gross effects, such as pit formation, are being considered. Previously reported yields of the order of 30 atoms/single ion (Ref. 6) indicate that some high-energy-density cascades occur at ion energies as low as 5.0 keV. Relatively large simulated pits are found at this energy in a model Cu(001)/Ar⟨001⟩ system, which here serves as a prototype for all fcc systems. Similar pits have been obtained with different ion energies and target orientations. The computed pits display many features observed experimentally, but the large pit shown in Fig. 1(e), approximately 1.8 nm in diameter, is below the threshold of visibility in the TEM. In the simulations, pits are seen as indicators of individual high-energy-density cascades for all potential functions, but neither high ion energies nor heavy ions are required for their formation.

Because these examples were designed to illustrate general properties of ion-bombarded fcc metals, the potential parameters used were chosen to bracket the entire range of plausible ion-atom functions. Pit formation is illustrated with two Born-Meyer ion-atom potential functions.[6] The R potential ($A = 59.874$ keV, $b = 7.200$ Å^{-1}) is very similar to the Cu/Ar^+ Moliere potential ($a_0 = 0.092$ Å) derived from surface semichanneling data by Shulga.[15] It gives good agreement with available experimental Cu/Ar^+ sputtering data. B-potential ions ($A = 71.303$ keV, $b = 4.593$ Å^{-1}) create much greater surface-deposited energies than would be expected in a Cu/Ar^+ bombardment, and are known to produce individual high-energy-density cascades similar to the spikes seen in Au/Sb^+, which has approximately the same mass ratio. Similar pits have been obtained with the "standard" Moliere potential ($a_0 = 0.1035$ Å), the "0.8" screening "modified"
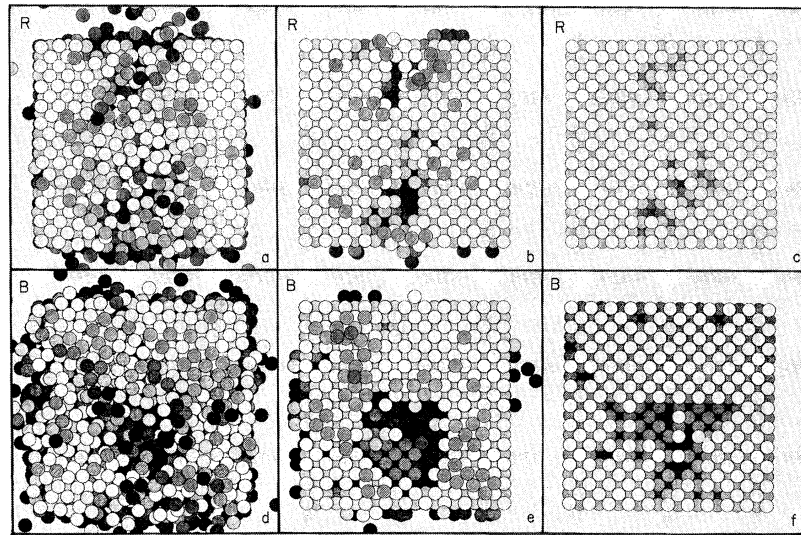
FIG. 1. These are top views of the model (001) crystallite. Masses and lattice constant are for Cu/Ar. The figure compares 5.0-keV trajectories run with the R [(a), (b), and (c)] and B [(d), (e), and (f)] potential functions: (a),(d) Condition of the target at the end of the sputtering event; (b),(e) condition of the target after cooling and coalescence; (c),(f) initial sites of the ejected atoms. Atoms appearing on the sides of the targets in (b) and (d) indicate that the targets are somewhat small for complete containment.

Moliere potential ($a_0 = 0.0828$ Å), and Shulga's value ($a_0 = 0.092$ Å).

The Cu/Cu atom-atom potential was the familiar compound POT-II ($A = 22.564$ keV, $b = 5.088$ Å^{-1}, $D_e = 0.4806$ eV, $\alpha = 1.405$ Å^{-1}, and $r_e = 2.628$ Å).[16] The targets were eight layers deep and contained 1764 particles. Although the targets are not large enough to totally contain a cascade, runs with both smaller and larger targets show only superficial differences in the pits created at comparable impact points.

Figure 1 shows top views of bombarded crystallites at the end of the atom ejection cascade ($\sim 5 \times 10^{-13}$ s), Figs. 1(a) and 1(d), and after cooling and coalescence ($\sim 10^{-11}$ s), Figs. 1(b) and 1(e), for each potential. These are high atom/single-ion events in a system where the computed (R potential) and experimental yield is about 4 atoms/ion at this ion energy. The pits obtained from the two potential functions are qualitatively similar, but the high-energy-density—potential crater shown in Fig. 1(e) is larger and deeper. Similar pits occur frequently with this potential function. Single large pits occur with the R potential, but an ion often produces a pair of pits of comparable size, see Fig. 1(b).

Note that pits exist in the precrystallized target, Figs. 1(a) and 1(d), but recrystallization clarifies their shapes. The crater formation process is complete as shown in Figs. 1(b) and 1(e), but re-

ordering by diffusion has not had time to occur.

In the figures, white atoms are near the original surface layer, and the degree of darkening indicates the distance above or below that layer. Shaded atoms on top of white atoms are more than 1.0 Å (in Cu) above the surface. In the recrystallized state, Figs. 1(b) and 1(e), these atoms form part of a new layer resting on the reformed surface. Fragments of a second layer also occur occasionally. These ordered layers of "target adatoms" form naturally, because there are attractive forces between the atoms, and require no special assistance by the program.

The original sites of the atoms ejected during these events are shown in Figs. 1(c) and 1(f). These vacancy patterns show some resemblance to the shape of the pits, see Figs. 1(b) and 1(e), but most of the ejected atoms came from the surface layer.

It is tempting to assume that the target adatoms were ejected from the pit and produced structure around the crater by mechanisms similar to the splashing which contributes to the rim surrounding a meteorite impact crater. A detailed analysis of the original positions of the target adatoms indicates that this hypothesis is incorrect. The target adatoms did not originate in the pit. Nearly all of them have net displacements of only one atomic layer, and were displaced from the surface layer by atom replacement-collision se-

quences; that is, sequences in which each atom is displaced into a neighbor's site.[17,18]

Replacement-collision sequences have been studied for many years,[17,18] but their relative importance as a damage producing mechanism is hard to assess from statistical cascade theory,[19] which studies the target in a state equivalent to the precooled trajectory, as shown in Figs. 1(a) and 1(d).

Figure 2(a) shows a 100-trajectory distribution of pit sizes from high-energy-density cascades (B potential), for $Cu(001)/Ar\langle001\rangle$ at 5.0 keV. The largest pit observed, Fig. 1(e), contains 304 vacancies. A hemispherical 300-vacancy pit would have a diameter of ~2.5 nm, near the limit of visibility in the TEM. At this ion energy, pits smaller than half that size are most common. This example produced 156 pits which contained less than 20 connected vacancies.

For comparison, the largest pit computed with the correct (Shulga) Cu/Ar^+ potential contains 180 vacancies. The largest using the K potential, one of those shown in Fig. 1(b), contains 130 vacancies. For both realistic potentials, most pits are smaller than 50 vacancies.
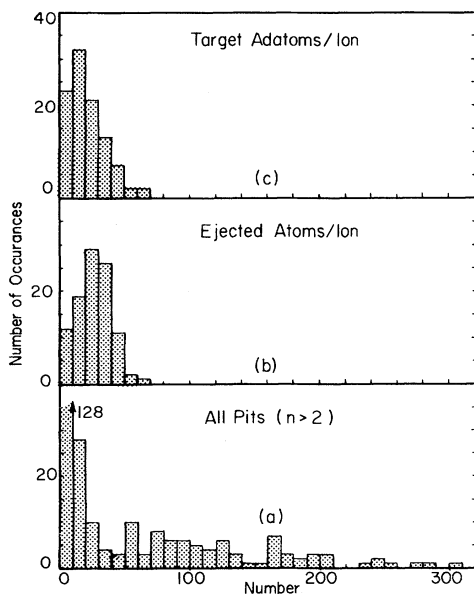

FIG. 2. Distribution functions for 100 trajectories at 5.0 keV on the (001) surface, with the B-potential function: (a) Distribution of pit sizes, including multiple pits from the same trajectory. A pit is defined as a connected set of vacancies. (b) Distribution of the number of atoms ejected per single ion, and (c) distribution of the number of "target adatoms" per single ion.

The B-potential distributions of ejected atoms and target adatoms also are shown in Fig. 2. Their average numbers are roughly comparable. There are many more vacancies than ejected atoms. The distribution of interstitial atoms is not shown because many of them will be annealed away later by diffusion. The average number of interstitial atoms generated is consistent with the number predicted by the Kinchin-Pease formula.

The poor correlation between the number of vacancies in the pit and the number of ejected atoms exists because there is little similarity between the mechanisms causing the ejection of atoms, which move parallel to and close to the surface, and the replacement-collision sequences deeper in the target which cause most of the pit vacancies. Pit formation does correlate with high ejected-atom yield, but the pit volume is not a measure of the yield from that ion.

These results, when combined with those previously reported, suggest that the essential difference between "low energy" and "high energy" sputtering is simply the fraction of trajectories which produce high yields, or pits. Under certain conditions, the largest pits will be observable. For other systems they will be below the level of observability.

In the simulations, both the maximum pit size and the probability that a pit of given size will form approach zero as the ion energy approaches the sputtering threshold. At somewhat higher ion energies they indicate that *all* atom-ejection experiments are the results of mixtures of low and high surface-deposited-energy events. The proportion of each type of event, and the distribution of pit sizes, is determined primarily by the target/ion system (the ion-atom potential function) and to a lesser extent by the target material and the ion energy.

[1]K. L. Merkle and W. Jager, Philos. Mag. 44, 241 (1981).

[2]K. L. Merkle and P. P. Pronko, J. Nucl. Mater. 53,

231 (1974).

[3]H. L. Bay. H. H. Andersen, W. O. Hofer, and O. Nielsen, Nucl. Instrum. Methods **133**, 301 (1970).

[4]P. Sigmund, Appl. Phys. Lett. **25**, 169 (1974).

[5]R. Kelly, Radiat. Eff. **32**, 91 (1977).

[6]D. E. Harrison, Jr., J. Appl. Phys. **52**, 4251 (1981).

[7]M. F. Dumke, T. A. Tombrello, R. A. Weller, R. M. Housley, and E. H. Arlin, to be published.

[8]D. E. Harrison, Jr., W. L. Moore, Jr., and M. T. Holcombe, Radiat. Eff. **17**, 163 (1973).

[9]D. E. Harrison, Jr., P. W. Kelly, B. J. Garrison, and N. Winograd, Surf. Sci. **76**, 331 (1978).

[10]D. E. Harrison, Jr., W. L. Gay, and H. M. Efforn, J. Math. Phys. (N.Y.) **10**, 1179 (1969).

[11]D. E. Harrison, Jr., to be published.

[12]R. P. Webb and D. E. Harrison, Jr., to be published.

[13]G. Carter, D. G. Armour, S. E. Donnelly, and R. P. Webb, Radiat. Eff. **37**, 1 (1978).

[14]D. E. Harrison, Jr., G. L. Vine, J. A. Tankovich, and R. D. Williams III, in *Applications of Ion Beams to Metals*, edited by S. T. Picraux, E. P. EerNisse, and F. L. Vook (Plenum, New York, 1974), p. 427.

[15]V. I. Shulga, Radiat. Eff. **62**, 237 (1982).

[16]D. E. Harrison, Jr., J. Appl. Phys. **53**, 4193 (1982).

[17]M. W. Thompson and R. S. Nelson, Proc. Roy. Soc. London, Ser. A **259**, 458 (1961).

[18]J. B. Gibson, A. N. Goland, M. Milgram, and G. H. Vineyard, Phys. Rev. **120**, 1229 (1960).

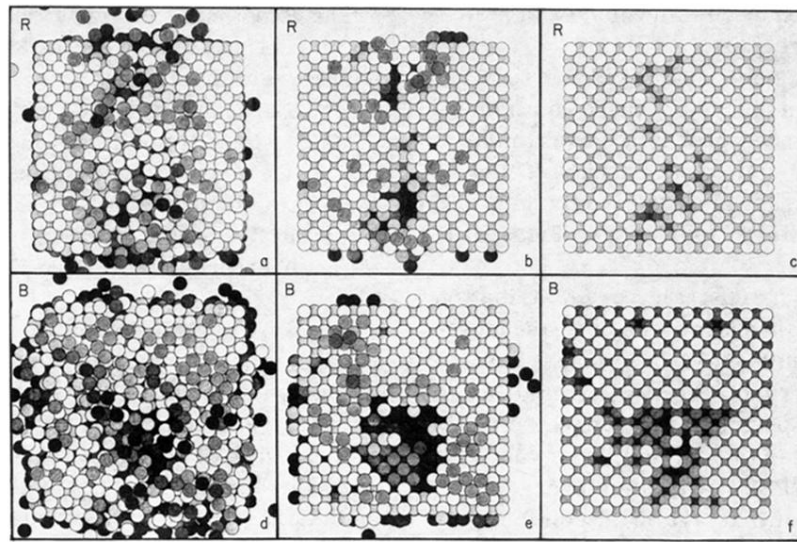[19]U. Littmark and W. O. Hofer, Nucl. Instrum. Methods **168**, 329 (1980).

FIG. 1. These are top views of the model (001) crystallite. Masses and lattice constant are for Cu/Ar. The figure compares 5.0-keV trajectories run with the R [(a), (b), and (c)] and B [(d), (e), and (f)] potential functions: (a),(d) Condition of the target at the end of the sputtering event; (b),(e) condition of the target after cooling and coalescence; (c),(f) initial sites of the ejected atoms. Atoms appearing on the sides of the targets in (b) and (d) indicate that the targets are somewhat small for complete containment.